




Cardan Shaft Load and Its Variation with Length

Jiri Struz^(✉) , Lukas Hruzik , and Jiri Havlik 

Faculty of Mechanical Engineering, Department of Machine Parts and Mechanism,
VSB – Technical university of Ostrava, 17. Listopadu 15/2172, CZ 708 33 Ostrava, Czech
Republic

jiri.struz@vsb.cz

Abstract. This paper follows the results of measurements carried out on trucks of different types. The emphasis is on the load on the cardan shaft and the variation of this load with its length. The effect of the angle between the shafts on the magnitude of the load torques is also investigated. In addition, attention is paid to the determination of the forces acting on the designed frame of the experimental equipment. These forces are used as input to the FEM analysis. FEM analysis considers the effect of these forces on the behavior of the frame as well as the magnitude of acceleration at specific locations. The evaluation is determined by combining the results obtained by the analytical approach and the FEM.

Keywords: Deflection angle · non-uniformity · transient structural analysis · acceleration · Fourier transform · length of cardan shaft

1 Introduction

In industrial practice, especially in the automotive industry, it appears that in applications in which a cardan shaft is used, negative vibrations occur at its second harmonic frequency. Measured data from different vehicles show that vehicles with a longer cardan shaft exhibit lower vibration. [1] The intensity of these vibrations depends mainly on the unevenness of the running, which is influenced by the deflection angle, commonly denoted as β . The uneven running can be eliminated theoretically by a simple modification so that the angles between the shafts of the driving and driven parts are the same. [2] This rule is often unattainable in practice, most often for building reasons or because of the suspension of following parts. As such, the running irregularity will further affect the time histories of angular velocities and accelerations [3], in addition, it will also influence the magnitudes of torques and force actions across the cardan shaft. It is also necessary to bear in mind the inertial effects of the individual parts. [4, 5] The reasons described above led to a reflection on how the length of the cardan shaft can influence vibrations and how to verify its influence. Based on these considerations, it was decided to construct an experimental device to vary the length of the cardan shaft, thereby changing the angles between the shafts β and thus also changing the force and moment action and ultimately the angular velocities and accelerations. The main focus

of this article will be the determination of the excitation forces acting on the frame of the mentioned experimental device, then the loads within the cardan shaft and their change depending on its length will be determined.

2 Materials and Methods

2.1 Determination of Excitation Forces

In this chapter, a large part of attention will be paid to the forces arising due to the unevenness of the Hook joint, especially at the location of the cardan shaft. The force and torque load on the cardan shaft are indicated on Fig. 1. The effect of the cardan shaft length will be assessed based on the variation of the forces acting on the frame of the experimental device at the foot of the electric motor and the tilting device with its length.

Assuming that the torque from the electric motor will be constant over time, so $T_1 = const.$, a time-varying torque $T_2(\gamma_1)$ will act on the intermediate shaft. The torque will be transmitted to the output shaft via another Hook joint, where act the torque $T_3(\gamma_1)$. The determination of the torques is based on the equality of the power on the input and output or intermediate shafts. [6] Similar problems are solved by i.e. [2–4].

$$T_1 \cdot \omega_1 = T_2 \cdot \omega_2(\gamma_1) \quad (1)$$

After modification, the following mathematical formulation for determining the torque can be obtained $T_2(\gamma_1)$:

$$T_2(\gamma_1) = \frac{T_1 \cdot [\sin^2(\gamma_1) \cdot \cos^2(\beta_1) + \cos^2(\gamma_1)]}{\cos(\beta_1)} \quad (2)$$

$$T_3(\gamma_1) = \frac{T_2 \cdot [\cos^2(\beta_2) \cdot \cos^2(\gamma_2) + \sin^2(\gamma_2)]}{\cos(\beta_2)} \quad (3)$$

In order to accurately determine the forces acting in the electric motor or tilting device mounting, it is also necessary to determine the additional torques $T_{b1}(\gamma_1)$ and $T_{b2}(\gamma_1)$. Using Eq. (4), (5) according to [8] we obtain a graphical time course, see Fig. 2.

$$T_{b1}(\gamma_1) = -T_1 \cdot \cos(\gamma_1) \cdot \tan(\beta) \quad (4)$$

$$T_{b2}(\gamma_1, \gamma_2) = T_1 \cdot \frac{\sin^2(\gamma_1) \cdot \sin(\beta)}{\sin(\gamma_2)} \quad (5)$$

Reliable determination of the additional torques can also be obtained using numerical methods.

It should be noted that some differences can be traced with the analysis performed in Ansys and with the relationships reported in [8]. By comparing Fig. 2 and Fig. 3 it can be seen that the time course of the additional torque $T_{b1}(\gamma_1)$ differ from each other. The fundamental differences are mainly in the magnitude of the torque amplitude and also in the angular frequency or period of the waveform. These differences are likely to be due to different initial conditions considered in the calculation, similar to the angular velocity described in the introduction. [7].

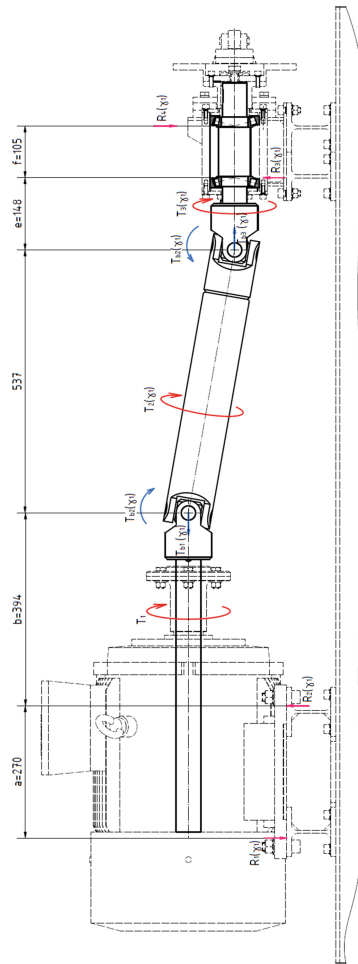


Fig. 1. Force and torque loads during the experiment.

2.2 Force Action via the Electric Motor Contact Surfaces

The text above describes the procedure for determining the torque across the entire cardan shaft. If the torque waveforms on the shaft are known, it is possible to determine the magnitudes of the forces acting on the frame of the experimental device. The force acting through the electric motor contact surfaces can be seen from Fig. 4, respectively Fig. 1. The forces loading the electric motor contact surfaces will be composed of two components, the first component of the force will be static and generated by the weight of the electric motor itself and the torque. The second component of the forces will be time-varying generated by the additional torques. The relationships for calculating the resulting forces acting at the contact surfaces of the electric motor with the frame are as follows:

$$F_1 = \frac{R_A}{2} - \frac{F_{max1} - F_{min1}}{2} \cdot \cos(\omega \cdot t + \theta_1) \tag{6}$$

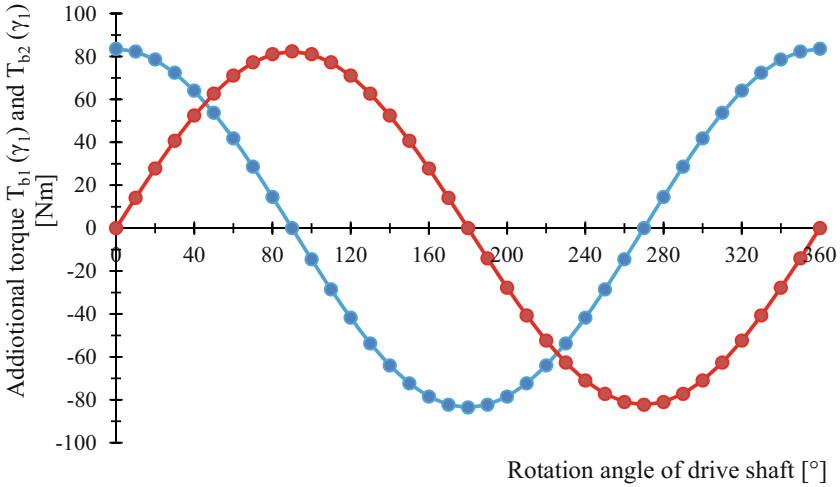


Fig. 2. Time course of additional torques $T_{b1}(\gamma_1)$ a $T_{b2}(\gamma_1, \gamma_2)$ – Eq. (4), (5).

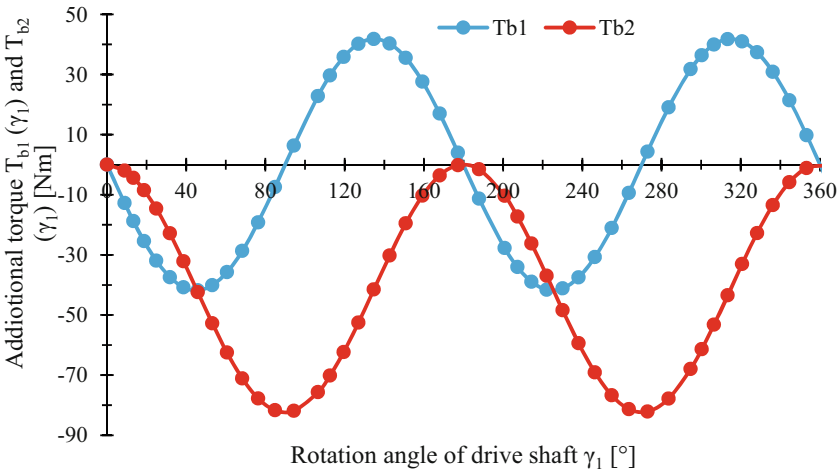


Fig. 3. Time course of additional torques $T_{b1}(\gamma_1)$ a $T_{b2}(\gamma_1)$ – FEM.

$$F_2 = \frac{R_B}{2} + \frac{F_{max2} - F_{min2}}{2} \cdot \cos(\omega \cdot t + \theta_2) \tag{7}$$

$$F_3 = \frac{R_B}{2} - \frac{F_{max3} - F_{min3}}{2} \cdot \cos(\omega \cdot t + \theta_3) \tag{8}$$

$$F_4 = \frac{R_A}{2} + \frac{F_{max4} - F_{min4}}{2} \cdot \cos(\omega \cdot t + \theta_4) \tag{9}$$

2.3 Determination of Excitation Forces in Tilting Device Bearings

The time course of the forces acting in the bearings of the tilting device is indicated in the following Fig. 5. The calculation procedure is similar to the previous case.

2.4 Comparison of Analytical Calculations and FEM

From the torque waveform, see Fig. 2 a Fig. 3 some differences are evident. These differences will certainly be evident in the results of the forces. A graphical comparison of these results is indicated in the figures below.

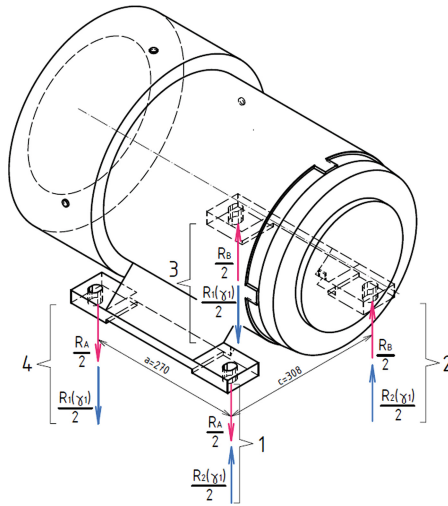


Fig. 4. Direction of forces acting on the frame via the electric motor contact surfaces.

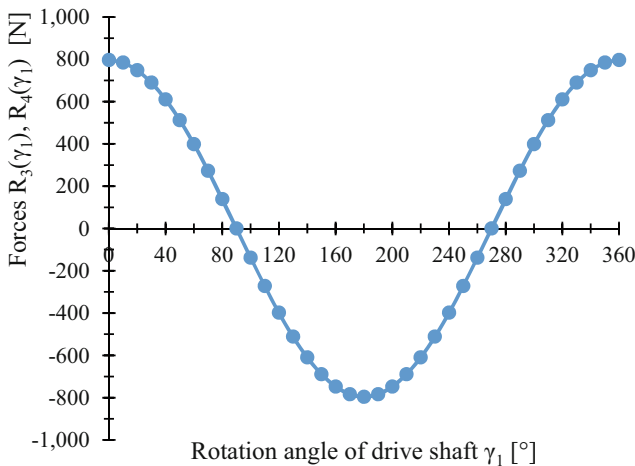


Fig. 5. – Time course of the forces acting in the bearings of the tilting device.

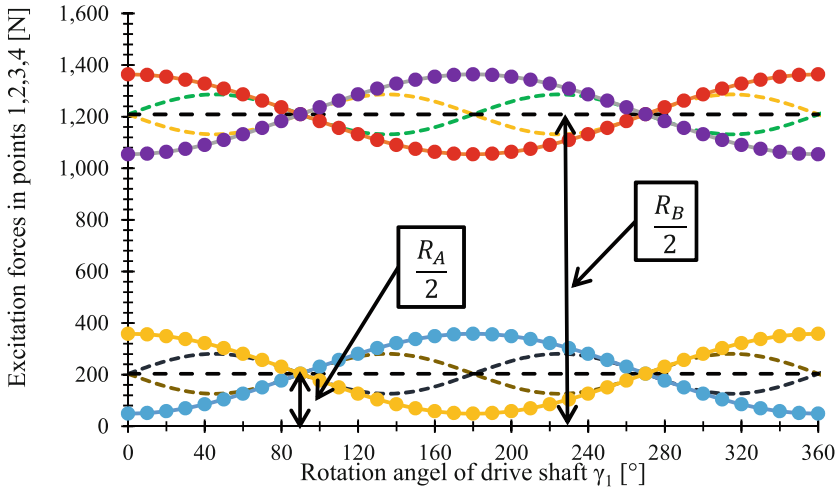


Fig. 6. – Graphical comparison of results obtained analytically or by FEM (Solid line shows results obtained analytically. Dashed line shows results obtained by FEM).

The differences described in the introduction of this subsection are reflected in the pattern of forces shown in Fig. 6. Since, the torque amplitude (Fig. 3) is smaller compared to the results on Fig. 2, this fact can also be seen in the force waveforms shown in Fig. 6. The frequency of the force is different as well. For the following calculations, analytical results are considered as their values are higher and are on the safety side.

2.5 Load Variation with Cardan Shaft Length

The purpose of this study is to specify exactly what effect the length of the cardan shaft has on its load or the load of the following components. The experimental device under consideration is designed to allow a change in the length of the cardan shaft by $\Delta l = 300\text{mm}$. In this way it is possible to achieve the arrangement indicated in Fig. 7. The figure also shows that changing the length will change the deflection angles, which will affect the resulting load.

The geometrical arrangement implies that the distance between Hooke's joints will vary between values 537 mm to 837 mm. If we scale distance by 100 mm, the deflection angles will correspond to the values $\beta = 8,4^\circ$; $\beta = 7,3^\circ$; $\beta = 6,4^\circ$. How the forces will change at the locations of the electric motor contact surfaces are shown in Fig. 8.

From Fig. 8 is obvious, that there is a reduction in the amplitude of the forces acting at the locations of the electric motor contact surfaces and also the tilting device. This phenomenon is caused by a geometric change in the drive arrangement, as the β angle decreases with increasing cardan shaft length.

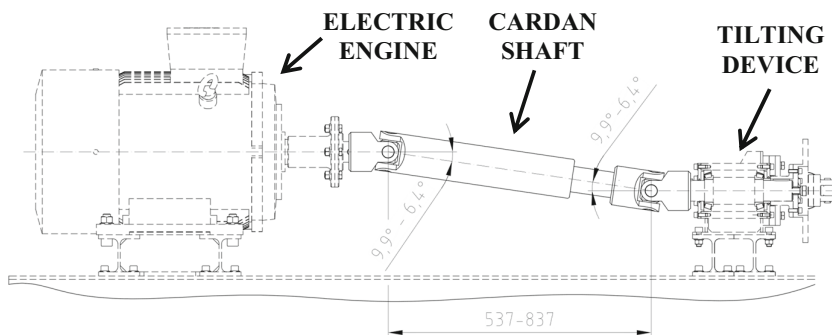


Fig. 7. Geometric arrangement considered during calculation.

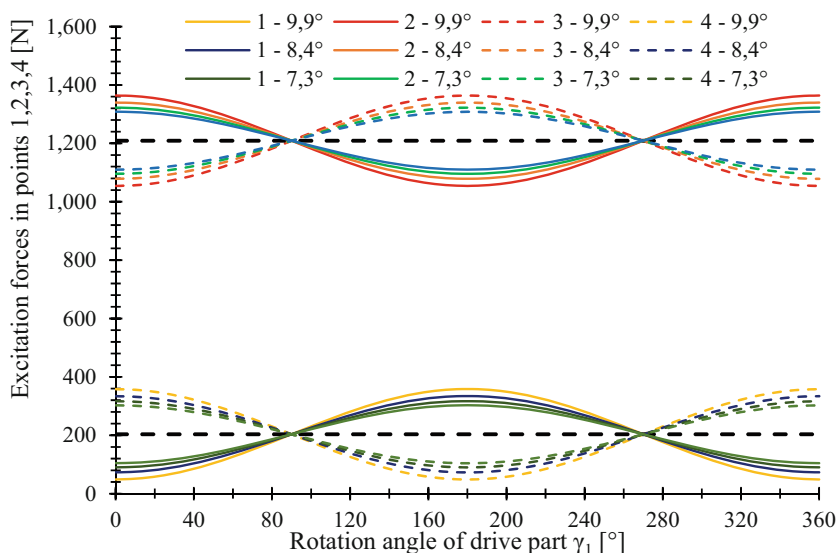


Fig. 8. Effect of the deflection angle on the course of forces at the electric motor footers.

3 Results and Discussing

In the previous chapter, the time-varying forces acting on the frame of experimental device were determined. On the basis of these calculations, a dynamic analysis was created to assess the influence of the length of the cardan shaft on the manifested vibrations, because these forces will change with the arrangement of the shaft or the change of its length.

Since the load forces vary with the length of the cardan shaft the results of this analysis can also be considered as a certain indicator of the influence of the length of the cardan shaft on the vibrations manifested. The following figures show the results of the simulation, with particular emphasis on the deformations, see Fig. 10 and the magnitude of acceleration at selected points in the frame, indicated in red in Fig. 9.

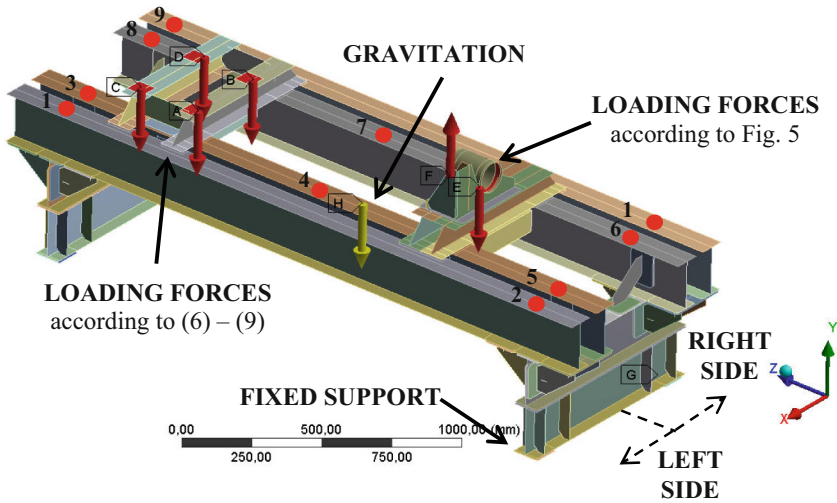


Fig. 9. Definition of initial conditions.

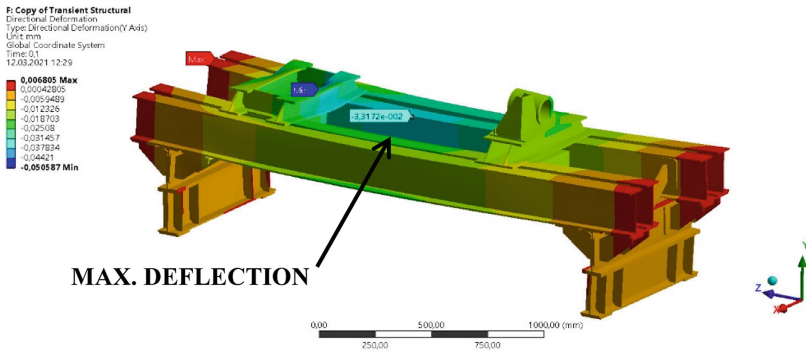


Fig. 10. Deformation of the frame in Y direction.

Figure 10 shows that the maximum deformation is achieved especially in the middle of the length of the IPE200 support profile and also at the location of the electric motor. Further attention is paid to the acceleration at the points marked in red. This method was chosen because vibration intensity is most often assessed by measurements, where vibration acceleration is most often examined. In the FEM analysis, data were obtained at all points marked in Fig. 9. The data from the FEM analysis were treated similarly to the measured data. In real measurements, in most cases the acquired acceleration data are evaluated by spectral analysis, respectively by the Fourier transform. The same approach was taken in this case. The data in the form of acceleration is viewed as data obtained from measurements that serve as input to the Fourier transform. The obtained waveforms in the frequency domain are then compared graphically at different cardan shaft lengths corresponding to Fig. 7. The red line represents a shift of the cardan shaft length by 300 mm, the blue line represents the initial state of the cardan shaft.

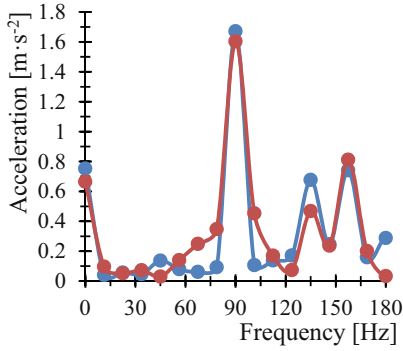


Fig. 11. Fourier transform for point 3 according to Fig. 7.

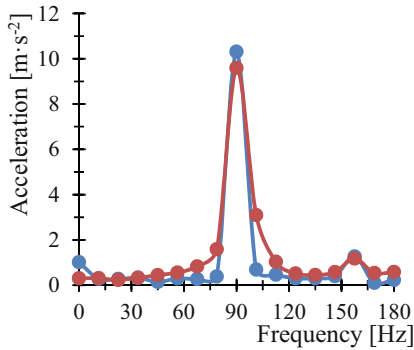


Fig. 12. Fourier transform for point 4 according to Fig. 7.

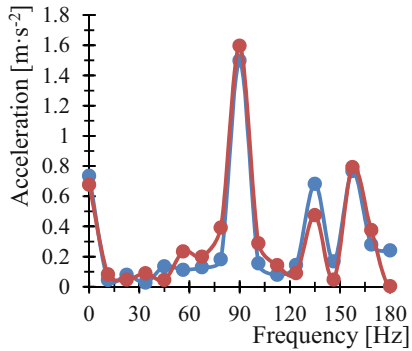


Fig. 13. Fourier transform for point 8 according to Fig. 7.

It can be seen from the above figures that the accelerations reach their highest intensity at point 4. By changing the length of the cardan shaft, the intensity is slightly reduced, but the intensity is significantly higher compared to the other points. This trend is visible

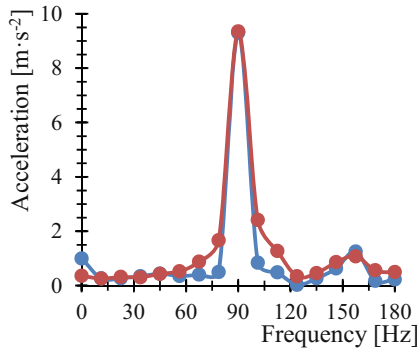


Fig. 14. Fourier transform for point 7 according to Fig. 7.

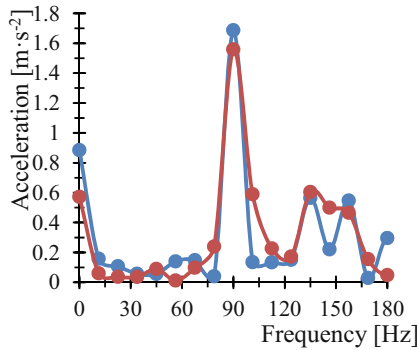


Fig. 15. Fourier transform for point 5 according to Fig. 7.

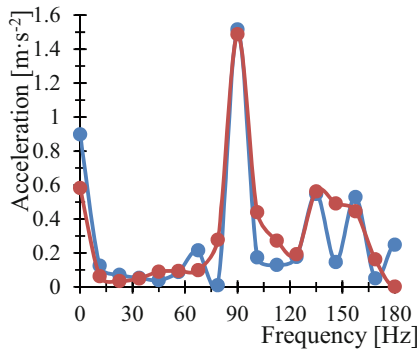


Fig. 16. Fourier transform for point 6 according to Fig. 7.

on the left part of the frame, respectively in points 3, 4, 5. On the right side of the frame, points 6,7,8, this trend is not apparent. There is a very slight increase in acceleration intensity (points 6, 8) or no significant change (point 7). The change in acceleration at

points 6,7 is so small that a calculation deviation cannot be ruled out. The fact that the acceleration value is highest at points 4 and 7 is due to the frame design itself and also to the fact that the IPE 200 profile reaches its highest deflection at this point, see Fig. 10. From the spectrums it can also be seen that the time course of acceleration at these points will be purely periodic. This is not the case at the edges of the frame, because the spectrums corresponding to points 3, 5, 6, 8 there is a sideband. The findings described above can be explained by the fact that with the length of the cardan shaft, the deflection angle decrease and also the load on the electric motor contact surfaces or tilting device is located. Therefore, decreasing acceleration values in points 3, 4, 5 can be expected. The fact that there are no significant changes in acceleration on the right side (points 6, 7) may be due to the fact that the forces (2, 3 - Fig. 4) on this right side are exerted by the electric motor contact surfaces, which are significantly higher than the forces (1, 4 - Fig. 4) between the frame and the electric motor contact surfaces on the left side. It can therefore be concluded that a change in the position of the forces of the tilting device does not have a significant effect on the acceleration at these points. In all these considerations, the influence of the frame design itself must also be kept in mind. The results in points 1, 2, 9, 10 are not shown here to save space. The trend of the results is consistent with the above results. The trends in points 1, 2 correspond to the trends in points 3, 4, 5, i.e. on the left-hand side. The trends in points 9, 10 correspond to the trends in points 6, 7, 8, i.e. on the right-hand side (Figs. 11, 12, 13, 14, 15 and 16).

4 Conclusion

This article responds to measured data on trucks with different types, which indicate that vehicles with longer driveshafts exhibit higher vibration. Based on this, a load analysis of the cardan shaft was carried out in this article. The torques on their individual shafts or additional bending moments were determined. The determination of moments was approached both by analytical method and by FEM. These moments are used as the basis for calculating the forces acting on the frame of experimental device. After expressing these forces, the influence of the deflection angle on their time course and magnitude was considered. The obtained results prove that with decreasing the deflection angle, the amplitude of the forces acting on the frame decreases. This is followed by a transient structural analysis of the experimental device frame, where these forces represent the boundary conditions. When evaluating the results on the frame, emphasis is placed on the resulting frame deformations over time and also on the acceleration of selected points/areas on the frame. Consequently, results were processed graphically based on the Fourier transform and compared. The graphic shows the behavior of the frame under load. At point 4, which corresponds to the point with the maximum deflection of the IPE200 section, it can be seen that the acceleration decreases with length. The magnitude of the acceleration is also highest at this point. By changing the length of the cardan shaft, the intensity is slightly reduced at points 3, 4 and 5. If we compare the acceleration values at these points, we find that the acceleration values at points 3 and 5 are very low. Another finding is that at these points the magnitude of acceleration decreases with the length of the cardan shaft, but at points 6, 7, 8 this trend is not apparent. At points 6, 8 is a very slight increase in acceleration intensity or no significant change (point 7).

From this, can be concluded that a change of the tilting device position does not have a significant effect on the acceleration at these points, because on the right side of frame acts higher forces than on the left side. Here it is necessary to consider the influence of the frame of experimental device design itself, which can significantly affect these values and must be taken into account in all considerations and interpretations of the results.

Acknowledgement. The research presented in this paper is an outcome of the project SP2021/31 “Experimental and computational methods for dimensioning of machine components 2021” funded by the Czech Ministry of Education, Youth and Sports.

References

1. STRUŽ, Jiří. *Analýza závislosti vibrací kardanové hřídele na její zástavbové délce* [online]. Ostrava, 2018 [cit. 2021–5–9]. Dostupné z: <http://hdl.handle.net/10084/129613>. Diplomová práce. Vysoká škola báňská - Technická univerzita Ostrava.
2. VLK, František. *Převody motorových vozidel*. Brno: František Vlk, 2006. ISBN isbn80–239–6463–1.
3. AN, K. a W. WANG. Transmission performance and fault analysis of a vehicle universal joint. *Advances in Mechanical Engineering* [online]. 2017, 9(5), 1–10 [cit. 2021–5–9]. Dostupné z: <https://doi.org/10.1177/1687814017707478>
4. VESALI, Farzad, Mohammad ALI REZVANI a Mohammad KASHFI. Dynamics of universal joints, its failures and some propositions for practically improving its performance and life expectancy. *Journal of Mechanical Science and Technology* [online]. 2012, 26(8), 2439–2449 [cit. 2019–7–6]. ISSN 1738–494X (Print) 1976–3824 (Online). Dostupné z: <https://doi.org/10.1007/s12206-012-0622-1>
5. ŠALINIĆ, Slaviša, Aleksandar VRANIĆ, Nešić NIKOLA D. a Tomović ALEKSANDAR M. On the torque transmission by a Cardan-Hooke joint. *FME Transactions*. 45. 2017, 45(1), 117–121. <https://doi.org/10.5937/fmet1701117S>. ISSN 14512092.
6. NĚMEC, Antonín, František BOHÁČEK a Vlastimil BUREŠ. *Části strojů III: Hřídele, ložiska a spojky*. Praha, 1964. Vysokoškolská skripta. Vysoké učení technické v Brně, Fakulta strojní.
7. STRUŽ, Jiří. *Teze disertační práce - Analýza vibrací kardanové hřídele pohonu nákladního automobilu*. Ostrava, 2020. Teze disertační práce. Vysoká škola báňská - Technická univerzita Ostrava. Vedoucí práce Doc. Ing. Jiří Havlík, Ph.D.
8. HUANG, Feng-Yun, Ding WEI a Lei SHI. Vibration Characteristic Analysis of the Cross-type Joint and Rzeppa Joint of the SS400 Transmission Shaft on Micro-vehicle. *Advances in Engineering Research: Proceedings of the Second International Conference on Mechanics, Materials and Structural Engineering (ICMMSE 2017)*. 2017, (102), 397–402. ISSN 2352–5401. Dostupné z: <https://doi.org/10.2991/icmmse-17.2017.66>

Open Access This chapter is licensed under the terms of the Creative Commons Attribution-NonCommercial 4.0 International License (<http://creativecommons.org/licenses/by-nc/4.0/>), which permits any noncommercial use, sharing, adaptation, distribution and reproduction in any medium or format, as long as you give appropriate credit to the original author(s) and the source, provide a link to the Creative Commons license and indicate if changes were made.

The images or other third party material in this chapter are included in the chapter's Creative Commons license, unless indicated otherwise in a credit line to the material. If material is not included in the chapter's Creative Commons license and your intended use is not permitted by statutory regulation or exceeds the permitted use, you will need to obtain permission directly from the copyright holder.

